Molecular Dynamics Simulations, Thermodynamic Analysis, and Experimental Study of Phase Stability of Zinc Sulfide Nanoparticles

Hengzhong Zhang,* Feng Huang, Benjamin Gilbert, and Jillian F. Banfield

Department of Earth and Planetary Science, University of California—Berkeley, 307 McCone Hall, Berkeley, California 94720

Received: July 18, 2003; In Final Form: September 9, 2003

A comprehensive study of the phase stability of ZnS nanoparticles was carried out using combined molecular dynamics simulations, thermodynamic analysis, and experimental investigations. Average surface energies of the sphalerite and wurtzite phases of zinc sulfide (ZnS) were calculated to be 0.86 and 0.57 J/m^2, respectively, using results from dynamics simulations of free faces of ZnS crystals at 300 K. Thermodynamic analysis, making use of the surface energy data, shows that smaller wurtzite nanoparticles are more thermodynamically stable than sphalerite. When the average particle size is ∼7 nm, the temperature for the transformation from sphalerite to wurtzite is 25 °C, dramatically lower than that observed in bulk material (∼1020 °C at 1 bar). The transformation from 3-nm sphalerite to wurtzite was simulated, and the activation energy was found to be only ∼5 kJ/mol. The very small activation energy may imply a different mechanism for the phase transformation in very small ZnS nanoparticles. Results of molecular dynamics simulations show that nanocrystalline sphalerite becomes more stable than wurtzite when sufficient water is adsorbed. Experimentally, when samples of synthetic ∼3-nm ZnS were heated in a vacuum over the range 350−750 °C, sphalerite transformed to wurtzite. However, there was no obvious conversion of sphalerite to wurtzite when samples were heated in air at 350 °C, probably due to the effect of chemisorbed water. The experimental data are consistent with the results of the thermodynamic analysis and molecular dynamic simulations, which indicate size dependence of ZnS phase stability and stabilization of sphalerite nanoparticles by water adsorption.

Introduction

Zinc sulfide is a semiconductor suitable for optoelectronic applications.[1] Its band gap is highly correlated with particle dimension[2] and with structure. However, the structural stability of nanocrystalline ZnS is very sensitive to the nanoparticle environment. Structural transformations in small ZnS nanoparticles can be caused by changes in the aggregation state[3] or adsorption of water.[4] Thus, to produce stable nanostructured ZnS materials that function properly in the operating atmosphere, it is necessary to understand how particle size and water moisture affect the phase stability.

At atmospheric pressure and room temperature, the bulk sphalerite phase (cubic structure) of ZnS is slightly more stable than the bulk wurtzite phase (hexagonal structure), with a free energy difference of ∼10 kJ/mol.[5] However, the entropy of wurtzite is ∼10 J/mol K higher than that of sphalerite. As a consequence, wurtzite and sphalerite are in equilibrium at 1020 °C and 1 bar (10^{-4} GPa)[5] and wurtzite is more stable at higher temperatures. At room temperature, cubic rocksalt structure ZnS becomes stable at pressures higher than ∼12 GPa.[6]

When the particle size of a substance is several nanometers or less, the particle dimension becomes a thermodynamic state variable that can significantly affect phase stability. A phase stability reversal can occur as a consequence of small particle size, if the stable bulk phase possesses a higher average surface energy, as in the nanocrystalline systems of TiO_2,[7] Al_2O_3,[8] and possibly nanocrystalline ZnS. It was reported that the sphalerite−wurtzite transition can be observed in nanoparticles at temperatures as low as 400 °C.[9]

The relative phase stability of nanocrystalline ZnS can be analyzed if the surface energies of all ZnS phases involved are known. However, the only reported value of the surface free energy of ZnS (∼0.05 J/m^2) is a measurement for sphalerite made using thin-layer wicking and contact angle techniques.[10] The value reported is unaccountably small compared to those of many other solid substances (∼1−4 J/m^2).[11]

Theoretical approaches, including empirical or semiempirical estimation,[12−14] first principles,[15] and lattice statics calculation,[16,17] have been widely used to predict surface energies. Nosker et al. used a charge compensation criterion to estimate the surface energies of various ZnS faces reconstructed.[12] By use of their method, the surface energies of sphalerite (111) and/or wurtzite (001) are ∼5 J/m^2. Assuming that the surface energy is approximately proportional to the dangling bonds per unit surface area, Yoshiyama et al.[13] and Tauson et al.[14] put forward equations to calculate the surface energies of various ZnS faces. From Yoshiyama et al., the sphalerite (111) face has a surface energy of ∼8 J/m^2, which is a factor of 2 higher than the highest reported values for most other solids. Tauson et al. gave a value of 1.0 J/m^2 for both the sphalerite (111) and wurtzite (001).[14] The average surface energies calculated using the frequently observed {111}, {110}, and {100} sphalerite and {001}, {100}, and {110} wurtzite surface energy estimates of ref 14 are 1.32 and 1.45 J/m^2, respectively. The predicted average surface energies for wurtzite are thus higher than for sphalerite, mainly due to the higher surface energy of {100} wurtzite compared to {100} sphalerite.

* Corresponding author. E-mail: heng@eps.berkeley.edu. Tel.: 510-643-9120.

10.1021/jp036108t CCC: $25.00
Published on Web 11/05/2003

The prediction that the average surface energy for sphalerite is lower than for wurtzite is inconsistent with experiments of these authors[18] and others.[9] For example, Tauson and Abramovich observed the change from sphalerite to wurtzite in fine particles (~10−120 nm) under hydrothermal conditions[18] and inferred that the surface energy of sphalerite is higher than wurtzite. Qadri et al. found that nanosphalerite can convert to nanowurtzite in a vacuum at temperatures much lower than 1020 °C,[9] suggesting that sphalerite possesses a higher average surface energy. The phase boundary between sphalerite and wurtzite of arbitrarily chosen morphologies was calculated as a function of the dimensions of the two phases at 600 and 1500 °C using the surface energies estimated in ref 14.[19] The transition temperature from nanocrystalline sphalerite to wurtzite cannot be determined from the plot. By use of an atomistic simulation method, Wright et al.[16] obtained surface energies of various faces of sphalerite, but wurtzite was not considered. The surface energy of a relaxed sphalerite (111) was calculated to be ~1.5 J/m^2.[16] Recently, Hamad et al. used lattice statics simulations to calculate the surface energy of ZnS.[17] For sphalerite (111) and the wurtzite (001), the calculated surface energies were each predicted to be ~0.9 J/m^2.[17]

In view of the literature information available, it is apparent that a set of reasonable and self-consistent values of surface energies for both sphalerite and wurtzite is needed for the thermodynamic analysis of the nanocrystalline ZnS system. This is one of the principal goals of the present work. We use molecular dynamics (MD) simulations at 300 K with periodic boundary conditions to find minimum-energy surface structures. The dynamic simulations explore configurations accessible at 300 K, guided by the interatomic potentials, and naturally incorporate important factors such as charge neutrality and energy convergence. By contrast, static simulations require manual input to attain geometries that would otherwise be inaccessible at 0 K. However, manual arrangement of surface atoms may create a surface structure not observed in a real crystal. According to the principles of semiconductor surface reconstruction,[20] the observed surface structure is the lowest free energy structure kinetically accessible under preparation conditions. The use of dynamic simulations therefore eliminates possible unnatural atomic arrangements.

We additionally use MD simulations of individual ZnS nanoparticles to test the phase stability predictions derived from theoretical surface energies, with and without the presence of surface water. Computational methods have been used to uncover diverse properties and spectacular behavior of individual or groups of nanoparticles.[21] For instance, using Monte Carlo simulations of maghemite nanoparticles, Iglesias and Labarta[22] found a reduction of the magnetic ordering temperature, spontaneous magnetization, and coercive field when the particle size is decreased. MD simulations are particularly suitable for large systems, such as nanoparticle aggregates during sintering. Averback et al.[23] found that Cu nanoparticles can rotate to find epitaxial orientations during sintering. Ogata et al.[24] found that enhanced surface diffusion in two anatase TiO_2 nanoparticles at high temperatures significantly promotes neck formation.

In the present work, MD simulations of single nanoparticles give specific, energy-minimized equilibrium structures, including surface reconstruction. When a nanoparticle is prepared with an initial sphalerite structure, a phase transition to the wurtzite structure is observed during the MD relaxation, confirming the prediction of a phase stability inversion at small sizes. Actual observations of phase transitions in MD may also provide detailed mechanism about the transformation.[25] Furthermore, we used single nanoparticle MD to investigate the structural consequences of surface water. The inclusion of surface species is relevant to all real-world applications of nanoparticles and is shown to significantly modify equilibrium structure and phase stability. Very few groups have managed to explicitly include surface interactions in structural predictions of nanomaterials.

TABLE 1: Surface Energies (J/m^2) of Faces of ZnS Dynamically Relaxed at 300 K

phase/face	100	110	111	001	average
sphalerite	2.56	0.39	1.84		0.86
	1.28[a]	0.65[a]	1.47[a]		1.00[a]
	1.21[b]	0.53[b]	0.94[b]		0.79[b]
wurtzite	1.00	0.28		1.52	0.57
	0.52[b]	0.49[b]		0.91[b]	0.59[b]

[a] Mean value from static calculations in ref 16. [b] Mean value from static calculations in ref 17.

Molecular Dynamics Simulations and Thermodynamic Analysis

Surface Energies of ZnS by Molecular Dynamics. We calculated the surface energies of various faces of ZnS at 300 K using MD simulations. The essential difference between this and previous works (e.g., refs 16 and 17) is that the free surfaces are relaxed dynamically at 300 K in this work (dynamic simulations) instead of using constrained geometric optimization with minimum energy criteria (static simulations at 0 K).

The crystal habit of ZnS depends on its crystallization environments (e.g., solution pH, sulfur content in solution, and electrochemical potential of the solution). Sphalerite crystals are often bounded by {111}, {1$\bar{1}$1}, {100}, {110} faces, or combinations of these.[26] For wurtzite crystals, the frequently observed faces are {100}, {110}, and {001} or combinations of these.[26] Our MD simulations focused on the representative faces for these forms, as listed in Table 1.

In the literature,[17,27,28] MD simulations of ZnS were done using different interatomic potential functions. We adopted the shell model[29] of ZnS by Wright and Jackson,[27] which is compatible with the MD simulation codes DL-Poly[30] and Shell-Dynamo[31] employed here. By use of the shell model, a Zn or S atom is treated as a core and a massless (or very light) shell that is connected by a spring, accounting for ionic polarity induced under a local electric field. The Zn and S atoms have the electrical charges of +2 and −2, respectively. The short-range non-Coulombic interaction between two atoms i and j takes a Buckingham form

$$u_{ij}\,(\text{short-range}) = A_{ij}\exp\left(-\frac{R_{ij}}{\rho_{ij}}\right) - \frac{C_{ij}}{R_{ij}^{6}} \qquad (1)$$

where u_{ij} is the interaction potential, R_{ij} the distance between atoms i and j, and A_{ij}, ρ_{ij}, and C_{ij} are three model parameters. An angle-bending form of three-body interactions is considered for nearest S−Zn−S atoms

$$u_{ijk} = \frac{1}{2}k_{ijk}(\theta - \theta_{ijk})^2 \qquad (2)$$

where u_{ijk} is the interaction potential; k_{ijk} a model parameter; θ the angle formed by atoms i (S), j (Zn, center), and k (S); and θ_{ijk} the equilibrium value of the angle (109.4°). For detailed values of the model parameters, the readers are referred to ref 27. By use of this model, the predicted lattice parameters of bulk sphalerite, wurtzite, and rock-salt phases of ZnS are no

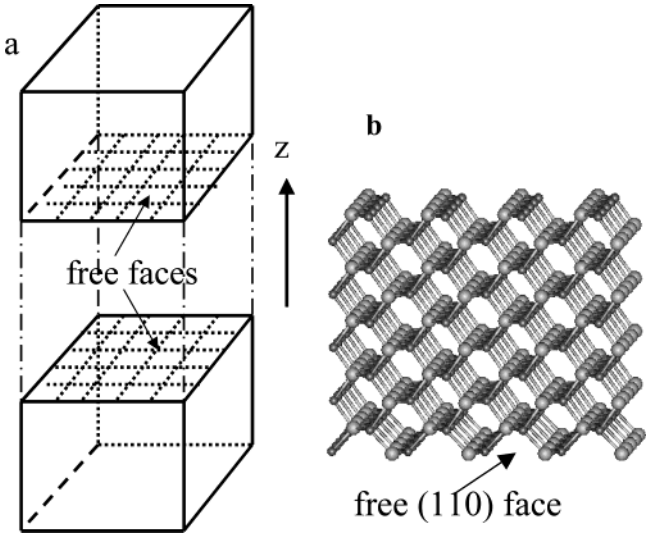

Figure 1. (a) A MD cell for dynamic simulation of the surface of bulk ZnS. The cell was cut from coordinates of a bulk ZnS crystal and rotated such that the desired free faces are oriented in the *z*-axis direction. A central slab was removed to form the two free faces (gridded), and the remaining faces (nongridded) of the cell satisfy periodic boundary conditions. The distance between the two free faces is ~10 nm, ensuring negligible atomic interactions between the two faces. (b) The upper slab of sphalerite after MD, viewed in the [1$\bar{1}$0] direction. The free (110) face lies at the bottom of the slab (bigger spheres, S atoms; smaller spheres, Zn atoms).

more than 0.1, 2.8, and 0.3% different from the literature values.[32] The predicted transition pressure from sphalerite to rock-salt phase at 300 K is 12 GPa, consistent with ref 6. The predicted energy of wurtzite is ~8 kJ/mol lower than that of sphalerite at 300 K and 1 bar, inconsistent with thermodynamic data[5] that show that the enthalpy of sphalerite is ~13 kJ/mol lower than that of wurtzite. Thus it would be inadequate to compare the thermodynamic phase stability of sphalerite and wurtzite nanoparticles by directly comparing their energies calculated by MD using the ZnS potential set. However, the relative magnitudes of the surface energies of various faces of sphalerite and wurtzite calculated using the same ZnS potential set should remain correct. This is because surface energy reflects the energy of a face relative to that of the bulk, determined primarily by the surface configuration of the face (e.g., the surface densities of surface atoms and dangling bonds) rather than by the rearrangement of atoms in the bulk. Thus, the surface energy values calculated using the chosen ZnS interatomic potential set can be used for following thermodynamic analysis, and this will be further justified by the agreement between the calculated phase relationships (below) and the experimental data (below). Since the rock-salt phase is stable only at high pressures, we did not include it in the thermodynamic analysis.

In the MD simulation of bulk ZnS a pair of free faces (e.g., sphalerite (111) and ($\bar{1}\,\bar{1}\,\bar{1}$)) is generated by removing a center slab from a bulk ZnS MD cell that satisfies the periodic boundary condition (Figure 1a). Both the top and bottom ZnS slabs are large enough (≥600 atoms) to simulate bulk ZnS using the periodic boundary condition on all faces except on the two free faces. The distance between the top and bottom ZnS slabs is sufficient (usually ~10 nm) that the atomic interactions between the two free faces are negligible. In the MD simulations of sphalerite (100), (110), and (111) and wurtzite (100), (110), and (001), the total number of atoms in the MD cells is 1024, 800, 1664, 1152, 720, and 600, respectively. All MD simulations were done in canonical (constant NVT) assemblies at 300 K with a time step of 0.5 fs for no less than 100 ps until the MD system was energetically relaxed. All computations were performed using Pentium PCs running Linux operating systems. In contrast to refs 12, 16, and 17, the relaxation and reconstruction of atoms on the free surfaces were achieved spontaneously during the dynamic simulation rather than by pure energy minimization and/or manual manipulation to avoid possible unphysical rearrangements. Figure 1b illustrates a relaxed slab of sphalerite with a free (110) face. The average Zn−S bond length in the surface layer (two atomic layers) is 2.30 Å, 0.05 Å shorter than that in the bulk. The surface energy of the relaxed face is calculated from the difference in the potential energy of the MD cell with free faces and that of a bulk ZnS of the same number of atoms, normalized by the sum of the surface areas of the free face pairs. The potential energy was calculated as an average value of about 20 instantaneous values, sampled at a 0.25-ps interval in the equilibrium period close to the end of a simulation. For instance, in the MD simulation of the sphalerite (110), the potential energy of the system (a total of 400 ZnS units) is −13 286 eV, while the potential energy of bulk sphalerite is −33.2656 eV/ZnS. The surface area of each (110) face is 412.0 Å^2. Thus, the surface energy of the (110) face = (−13 286 − (33.2656 × 400))/(412.0 × 2) = 0.025 eV/ Å^2 = 0.39 J/m^2. Table 1 summarizes the surface energies of various faces of ZnS obtained from the MD simulations.

To minimize the total free energy, the equilibrium crystal form develops so that the crystal is bounded by low surface energy faces. For two faces *i* and *j* at equilibrium, $A_i\gamma_i = A_j\gamma_j = \mu$, where μ is the excess chemical potential of surface atoms relative to interior atoms. A face (*i*) with higher surface energy (γ_i) consequently has a smaller surface area (A_i), which is inversely proportional to the surface energy. Accordingly, the average surface energy (γ) of the crystal, weighted by the surface area, is

$$\gamma = \frac{\sum_{i=1}^{n} A_i\gamma_i}{\sum_{i=1}^{n} A_i} = \frac{\sum_{i=1}^{n} \frac{\mu}{\gamma_i}\gamma_i}{\sum_{i=1}^{n} \frac{\mu}{\gamma_i}} = \frac{n}{\sum_{i=1}^{n} \frac{1}{\gamma_i}} \qquad (3)$$

where *n* is the number of faces under consideration. Each crystal has its own surface energy and a crystal can be bounded by an infinite number of face types. Thus, we confine ourselves to the frequently observed sets of ZnS forms (Table 1) and calculate the corresponding average surface energies according to eq 3. Consequently, we calculate that the average surface energy of sphalerite is ~0.3 J/m^2 higher than that of wurtzite.

For sphalerite {100}, the present result differs appreciably from values previously reported.[16,17] In the works of ref 16 and 17, some surface atoms were intentionally moved to other places in order to remove the surface polarity for the convergence of the atomistic calculations. By contrast, in our dynamic simulations, atoms diffuse naturally to appropriate positions with the kinetic energy provided by the thermal bath. Analysis of the free (100) surface after MD shows that the surface was able to relax to a kinetically attainable minimal-energy state at 300 K by both surface relaxation (shortening in bond length in the surface layer) and reconstruction (reposition of atoms on or near the surface by diffusion). All surface structures are given in Figures S.1−S.3, Supporting Information. This coincides with the principle that the surface structure observed is the lowest free energy structure kinetically accessible.[20] The generation of the vacancies near the (100) surface is a result of the reconstruction attempting to reduce the surface polarity.[20]

The experimental temperature dependence of the surface reconstruction of the ZnS (100) face is not available, but data is available for ZnSe (100).[33] As the annealing temperature increases from ~150 to ~550 °C, the reconstruction of the ZnSe (100) surface changes from (1 × 1) to (2 × 1) and to c(2 × 2). The ZnS (100) surface predicted from static calculations[16] does not coincide with these experimentally observed reconstructions. Furthermore, the calculated Wulff shape of a cubo-octahedral sphalerite crystal using the surface energy values from the present work is closer to that found in the nature[26] than that calculated using the values from ref 16 (Figure S.4, Supporting Information). Hence, the surface reconstructions and surface energies predicted by dynamic calculations may be more representative of real crystals.

For simplicity, in this work the average surface energy of ZnS will be regarded as independent of temperature, considering that the temperature coefficient of the surface energy of ZnS is in the order of 10^{-4} J/m^2 K.[14]

Thermodynamic Analysis. Previously, we made a thermodynamic analysis of the phase stability of nanocrystalline titania.[7] Both surface energy and surface stress were found to play significant roles in the phase stability of nanocrystalline titania. Following ref 7, the change of the molar standard free energy ($\Delta G°$) from nanocrystalline sphalerite to nanocrystalline wurtzite is

$$\Delta G^{o} = \Delta G^{o}(\infty) + \frac{2(2t+3)M}{D}\left(\frac{\gamma_w}{\rho_w} - \frac{\gamma_s}{\rho_s}\right) \qquad (4)$$

In eq 4, $\Delta G°(\infty)$ is the standard free energy change from bulk-(∞) sphalerite to bulk wurtzite, M the molecular weight of ZnS (97.46 g/mol), γ the surface energy (which is approximated as the surface free energy in this work), t the ratio of surface stress to surface energy ($t \approx 1$ is assumed in the work), D the average diameter of nanoparticles, and ρ the density of ZnS (we take $\rho = 4.1 \times 10^6$ g/m^3 for both sphalerite and wurtzite).[32] The subscripts w and s stand for wurtzite and sphalerite, respectively.

The $\Delta G°(\infty)$ data between 298 and 1293 K are available from ref 5. A plot of $\Delta G°(\infty)$ vs temperature (T in K) shows a very good linear relationship that can be represented by our following least-squares regression equation (regression coefficient = 0.92).

$$\Delta G°(\infty; \text{kJ/mol}) = 13.3325(\pm 0.0144) - 0.01034(\pm 0.00002)T \qquad (5)$$

In the equation, the numbers in the parentheses are the standard deviations.

Inserting values of t, M, ρ, and γ in Table 1, as well as eq 5 into eq 4, we obtain

$$\Delta G^{o}(\text{kJ/mol}) = 13.3325 - 0.01034T - \frac{68.935}{D} \qquad (6)$$

where D is in nm. Figure 2a shows the variation of $\Delta G°$ with particle diameter D at 300 K. At $D < \sim 7$ nm, $\Delta G° < 0$, wurtzite becomes more stable than sphalerite. The transition temperature for the transformation from nanocrystalline sphalerite to wurtzite can be derived from eq 6, by setting $\Delta G° = 0$, giving

$$T_t = 1289.4 - \frac{6666.8}{D} \qquad (7)$$

Thus, the temperature vs particle size phase diagram can be calculated from eq 7, as shown in Figure 2b. The transition temperature decreases dramatically once the particle size decreases below ~20 nm. For comparison, the phase boundary using the surface energies of ref 17 (Table 1) was also calculated (dotted line in Figure 2b).

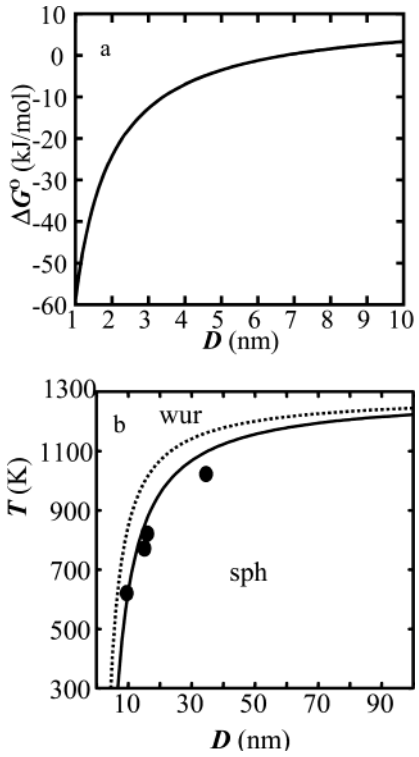

Figure 2. (a) The variation with particle diameter of the free energy difference between nanocrystalline wurtzite (wur) and sphalerite (sph) at 300 K. (b) The temperature−particle size phase diagram for nanocrystalline ZnS system. In (b), experimental data points from present work are shown as filled circles (see text); the solid line and the dotted line are the phase boundaries calculated using the surface energies from the present work and ref 16, respectively (Table 1).

MD Simulation of a 3-nm Sphalerite at 300 K. ZnS nanoparticles synthesized from an aqueous solution are about 3 nm in diameter (see Experimental Section, below). According to Figure 2b, at $D = 3$ nm, wurtzite is more stable than sphalerite, which we tested by energy minimization of a 3 nm diameter sphalerite nanoparticle, cut from bulk sphalerite. The starting configuration is shown in Figure 3a and contains 360 ZnS molecular units. The MD simulation was done in a canonical ensemble at 300 K with a time step of 0.5 fs. The energy evolution of the MD simulation is given in Figure 4, which shows a rapid initial relaxation of the initial configuration. After about 360 ps, the system reaches a transition state (a local energy maximum), after which the energy decreases and eventually approaches to a steady value. The total MD simulation time is ~3.6 ns. A snapshot of the final structure of the nanoparticle is shown in Figure 3b. Evidently, the wurtzite structure was formed, as indicated by the characteristic hexagonal [001] channels. According to Figure 4, the relaxed wurtzite structure is about 10 kJ/mol more stable for this size of nanoparticle than sphalerite, close to the value (~13 kJ/mol) given by the thermodynamic analysis shown in Figure 2a. The activation energy for the transformation from 3-nm sphalerite to wurtzite is ~5 kJ/mol (Figure 4). The very small activation energy in nanoparticles may indicate that the mechanism for the phase transformation in very small ZnS nanoparticles differs from that for bulk transformation. Inspection of the MD trajectories indicates that the nanoparticle transformation is driven by surface reconstruction, which propagates into the interior and throughout the entire particle. Hence, the transformation occurred following surface nucleation, with a lower

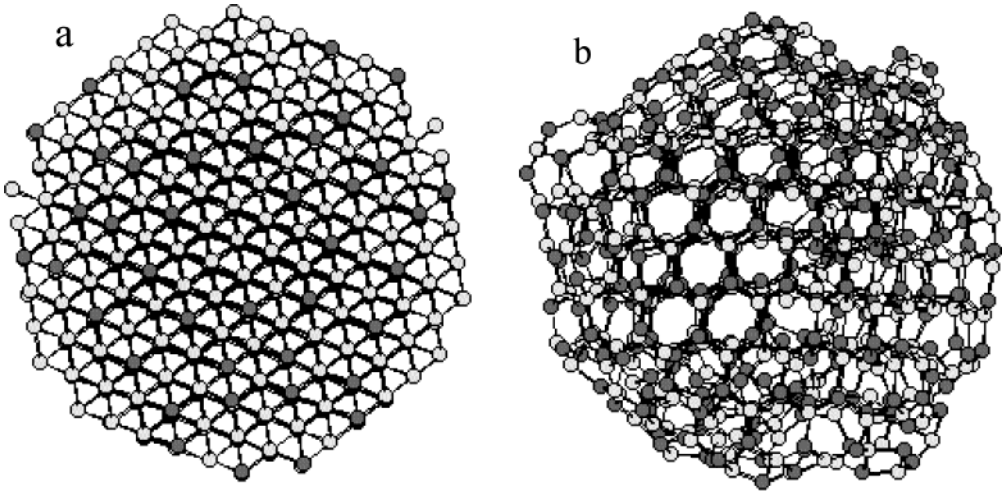

Figure 3. (a) A 3-nm sphalerite particle viewed along the [111] direction, the starting configuration for MD simulation. (b) The energy-minimized structure obtained by the MD. The [001] hexagonal channels of wurtzite can be easily seen in (b). Dark gray spheres, Zn atoms; light gray spheres, S atoms.

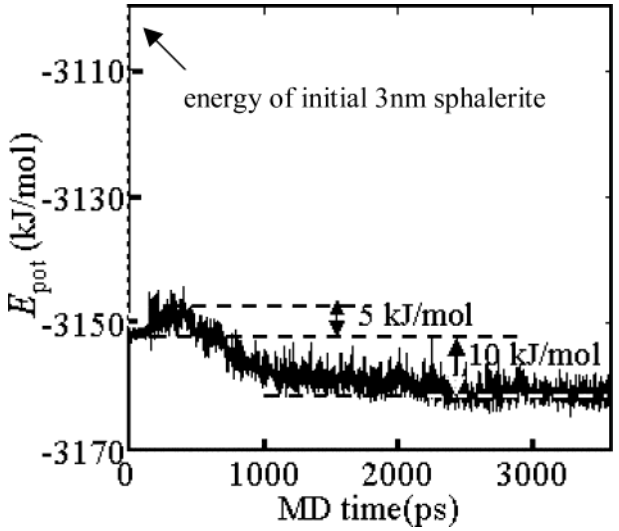

Figure 4. Potential-energy evolution during MD at 300 K of a 3-nm, initially sphalerite particle. The quick relaxation of the initial structure is indicated by the rapid decrease in the potential energy shown by the dashed line on the left ordinate.

activation energy than bulk nucleation. Experimental observation of aggregation-induced transformations in ZnS nanoparticles at room temperature[3] supports the concept that there are low activation barriers for structural changes in this system.

MD Simulation of the Influence of Water Adsorption on Phase Stability of Nanocrystalline ZnS. Water is ubiquitous at and near the Earth's surface. In this work, we used MD simulations together with experiments (see below) to investigate the influence of water adsorption on the phase stability of ZnS nanoparticles. In contrast to the earlier analysis of bulk surfaces of ZnS in a vacuum, the effects of ZnS−H_2O interactions on the structure of nanoparticles were simulated directly by MD simulations of single nanoparticles. The MD simulations are important because strong chemical interactions may occur between nano-ZnS and water that cannot be appropriately interpreted using the concepts of surface energy.

The interatomic potential functions used for ZnS are from ref 27. There are abundant water models used for MD simulations in the literature.[34] The shell water model,[35] the simple point charge (SPCE) water model,[36] and the central force (CF) water model[37] were tested in the MD simulations of water adsorption on a ZnS nanoparticle in this work. The interactions between atoms of ZnS and H_2O were assumed to be purely electrostatic, except those between Zn and O and between S and H, which both include additional short-range non-Coulombic interactions of the Buckingham equation form. The short-range interaction between Zn and O follows that in ref 38, and that between S and H was obtained by fitting the Buckingham equation to the ground-state potential energy surfaces of H_2S gas calculated from first principles[39]

$$u_{S-H}(\text{short-range}) = 15644.3 \exp\left(-\frac{R_{S-H}}{0.1565}\right) - \frac{21.289}{R_{S-H}^{\ 6}} \quad (8)$$

where u is in eV and R in Å. By use of the interatomic potential functions for the ZnS−H_2O system selected or obtained above, MD simulation runs revealed that only the shell water model[35] is compatible with the shell ZnS model.[27] With the SPCE water model, a spherical ZnS nanoparticle is highly deformed in the MD simulation; while with the CF water model, water molecules highly dissociate on the surface of a ZnS nanoparticle (Figures S.5 and S.6, Supporting Information), both unrealistic outcomes. With the shell water model, the shape of a spherical ZnS nanoparticle remains essentially spherical (in agreement with transmission electron microscope studies)[40] and water molecules on the ZnS surface do not dissociate (Figure S.7, Supporting Information). Thus, the shell water model was chosen for the MD simulation of ZnS−H_2O interactions. For a detailed description of the shell water model, see ref 35.

In the simulations, initial 2-, 3-, and 5-nm ZnS nanoparticles were constructed from the coordinates of bulk sphalerite and wurtzite. A thin spherical shell of water molecules corresponding to ~1, 3, and 5 H_2O/nm^2 ZnS was cut from equilibrated bulk water coordinates and placed over the surface of a ZnS nanoparticle. A MD simulation was done in a canonical assemble at 300 K at a time step of 0.5 fs for about 100 ps or until the potential energy of the system reached a steady value without a loss of the initial phase. Adsorption of water molecules on the ZnS nanoparticle can be readily seen in a movie generated from the MD simulation trajectory file.

The relative phase stability of nanocrystalline sphalerite and wurtzite at the same particle size and water surface coverage can be compared using their total energies (including the contributions from ZnS and those from the ZnS−H_2O interactions), as in this case both the sphalerite-water system and the wurtzite-water system have approximately equal numbers of Zn

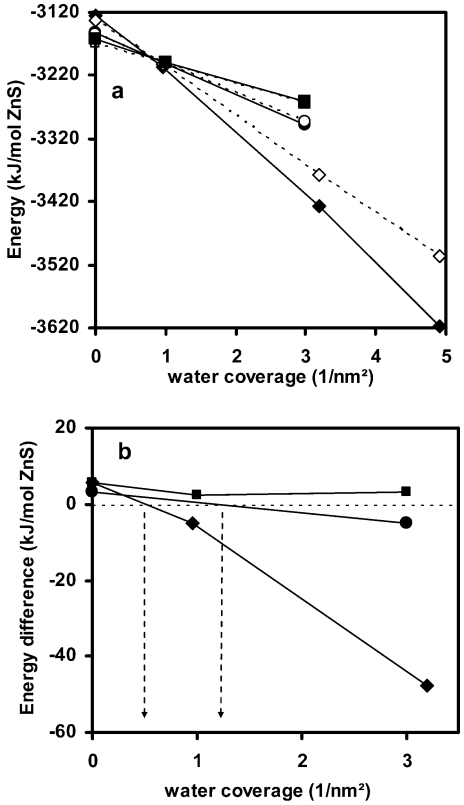

Figure 5. Variation of the energy of a ZnS nanoparticle (a) and the energy difference between sphalerite and wurtzite (b) with the amount of water adsorbed. Diamonds, 2 nm; circles, 3 nm; and squares, 5 nm. In (a), sphalerite, solid lines and closed points; wurtzite, dashed lines and open points. Results show that the particles become more stable with increasing particle size (at zero water content), that addition of water increases particle stability, and that the effect of water adsorption on the phase stability is greatest for the smallest particles.

and S atoms and water molecules. The energy of each phase is calculated from

$$\begin{aligned} &E(\text{ZnS with } H_2O \text{ contribution}) \\ &\quad = E(\text{ZnS self}) + E(\text{ZnS}-H_2O \text{ interaction}) \\ &\quad = (E(\text{ZnS self}) + E(\text{ZnS}-H_2O \text{ interaction}) + \\ &\qquad E(H_2O \text{ self})) - E(H_2O \text{ self}) \\ &\quad = E(\text{ZnS}-H_2O \text{ whole system}) - E(H_2O \text{ self}) \quad (9) \end{aligned}$$

In the equation, $E(H_2O$ self) is the energy of the hollow water shell when the nanoparticle has been removed. The two terms on the right side can be obtained from the MD simulations. Thus the energy on the left side can be calculated.

Figure 5a shows the variation of the energy of ZnS with the amount of water adsorbed. In Figure 5b, the variation of the energy difference between sphalerite and wurtzite phases is plotted. It is seen that for 2−5 nm ZnS nanoparticles, wurtzite has a lower energy than sphalerite prior to water adsorption. However, for 2- and 3-nm ZnS nanoparticles, even with minor water adsorption, the energy of sphalerite is lower than that of wurtzite (at a water coverage greater than ∼0.5 and ∼1.2 H_2O molecules /nm^2 ZnS, respectively). The higher the water coverage, the lower the energy of sphalerite compared to wurtzite. In 5-nm ZnS nanoparticles, wurtzite remains more stable than sphalerite even at ∼3 H_2O molecules/nm^2 ZnS. More water adsorption is needed to stabilize sphalerite relative to wurtzite in 5-nm ZnS nanoparticles (the precise amount of water needed has not been determined).

On the basis of the general tendency exhibited in Figure 5, we infer the following. At a certain temperature, and in the region where wurtzite is stable in a vacuum (e.g., <∼7 nm at 300 K according to Figure 2b), the amount of adsorbed water needed to make nanocrystalline sphalerite more stable than wurtzite should increase with increasing ZnS particle size. However, when the particle size approaches the value at which both phases reach the same stability in a vacuum, the amount of water needed should pass through a maximum value and then decrease.

A point to note in Figure 5: at the same water surface coverage, a smaller ZnS nanoparticle has lower energy than a bigger one. This does not mean a smaller ZnS nanoparticle is more stable than a bigger one because the amount of water molecules and the number of ZnS atoms are different in the two particles, i.e., they have different chemical compositions, so the normalized energies are not directly comparable. In the calculation of the energy, a smaller ZnS nanoparticle has fewer ZnS molecular units (roughly proportional to D^3) to normalize the negative $E(\text{ZnS}-H_2O$ interaction) contribution (roughly proportional to $-D^2$), and so its normalized ZnS$-H_2O$ contribution is more negative (roughly proportional to $-D^2/D^3 = -1/D$), thus its energy E(ZnS with H_2O contribution) appears lower than that of a bigger nanoparticle.

Experimental Section

Experiments were carried out in parallel with the MD simulations and the thermodynamic analysis in order to test the theoretical results. Nanocrystalline ZnS samples were synthesized, and the samples were heat treated in a vacuum or in air at various temperatures. The phases present were identified using X-ray diffraction (XRD), and the average particle size and the phase content were calculated from the XRD data. In the work, XRD experiments were performed using a Scintag PADV diffractometer with Cu Kα radiation (35 kV, 40 mA). Transmission electron microscopy (TEM) observation of the microstructures was done using a Philips CM200 high-resolution transmission electron microscope operated at 200 kV.

Synthesis of Nano-ZnS Samples. Mercaptoethanol (0.78 mL) was added dropwise into a continuously stirred 1 L solution of zinc chloride (10 mM), forming a homogeneous mixture. The acidity of the solution was adjusted to pH = 10.2 using a 1 M NaOH solution. Over a 2 h period, 1 L of sodium sulfide solution (10 mM) was added dropwise into above continuously stirred solution. The mixture was stirred for another 2 h. A homogeneous stable dispersion was formed. The reaction mixture was dialyzed for 40 h using 10-kDa dialysis tubes in order to remove excess ions. The dialyzed solution was further mixed with a 100-mL mixture of methanol−propanol (1:2 in volume) and was stirred thoroughly. The ZnS precipitates were separated from the solution by centrifuging and were further dried in a vacuum to obtain ZnS powder.

Figure 6a shows the TEM image of the as-synthesized raw ZnS material. The majority of the material is ∼3-nm sphalerite particles, but lattice fringe periodicities normal to [001] wurtzite indicate a very small amount of wurtzite is present (data not shown). Curve 1 in Figure 7a, b shows the XRD pattern of the as-synthesized ZnS sample. The broadening of the sphalerite (111) or (220) XRD peaks analyzed using the Scherrer equation (eq 10)[41]

$$D = \frac{0.90\lambda}{\text{fwhm} \cos\theta} \quad (10)$$

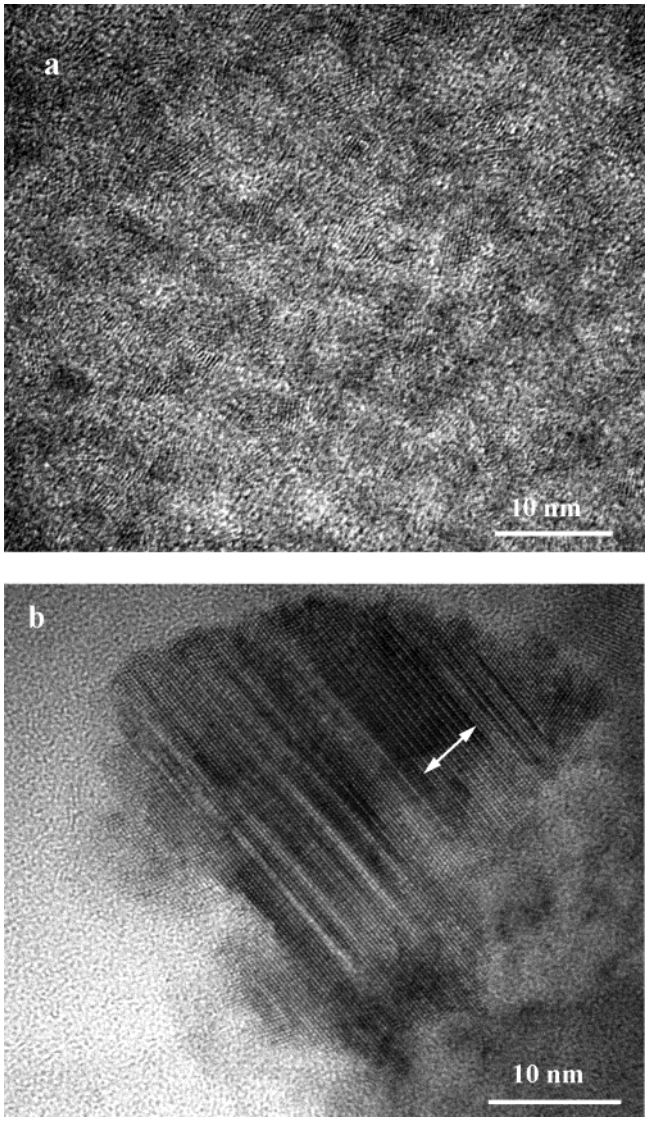

Figure 6. TEM images of as-synthesized raw ZnS material (a) and a ZnS nanoparticle in the sample heated under vacuum at 500 °C for 48 h (b). The arrow in (b) indicates the location of a region of the wurtzite phase.

indicated that the average particle size of ZnS is ~1.5 nm. In eq 10, λ is the wavelength of Cu Kα radiation (1.5418 Å), 0.90 is the Scherrer constant, θ is the Bragg reflection angle, and fwhm is the full width at half-maximum intensity of the chosen XRD peak. The difference between the XRD size and the TEM size for the ultrafine raw ZnS sample is due to strain, either throughout the nanoparticles or at its surface. When nanoparticles are bigger than ~5 nm, the average particle size given by the Scherrer equation is close to that estimated by TEM.

Heat Treatment of Nanocrystalline ZnS Samples. About 40 mg of the initial ZnS nanomaterial was sealed under vacuum in silica tubes about 10−15 cm in length and 8 mm in diameter (the vacuum pressure was $\sim 10^{-6}$ Torr). Eight tubes were then sequentially heated in an electric furnace at temperatures ranging from 350 to 750 °C for different periods and then quenched to room temperature in air. The product formed in each sample was examined by XRD, as shown in Figure 7a. Formation of wurtzite occurred rapidly upon heating in a vacuum, as shown by the appearance of wurtzite (100), (101), (102), and (103) peaks at every temperature. Figure 6b shows a TEM image of a sphalerite nanoparticle partially transformed to wurtzite after heating the raw sample at 500 °C for 48 h. This particle exhibits a very complex structure, including stacking faults and twins. In every case of partially reacted sphalerite examined, the wurtzite formed in the central region of nanoparticles rather than at the surface terminations of the *c* axis. In contrast, no significant wurtzite formation was detected in a ZnS sample heated in air at 350 °C for 2 h (Figure 7b). A small peak at ~28.6° is attributed to wurtzite (100) (TEM data show minor wurtzite in the starting material, but the peaks cannot be resolved by XRD). This sample was heated for another 21 h in air. The XRD pattern (Figure 7b) shows coarsening of sphalerite but no increase in wurtzite content. Other characteristic peaks of wurtzite (e.g., 101, 102, and 103) are virtually invisible.

Correlation between Wurtzite Content and XRD Peak Area Fraction. To calculate the wurtzite content of a ZnS sample containing both sphalerite and wurtzite, a standard curve depicting the relationship between the wurtzite content and the XRD peak areas is needed. This relationship can be obtained from XRD data (Figure 7c) of standard samples consisting of pure sphalerite and pure wurtzite. Sphalerite powders from Aldrich Chemical Co., Inc. (Milwaukee, WI; <10 μ, 99.99% purity), were subjected to lengthy hydrothermal treatment at 250 °C and then washed and dried to obtain pure sphalerite. Pure wurtzite was produced by heating the sphalerite in a vacuum-sealed silica tube at 1100 °C for 9 h, followed by rapid cooling in air. In the XRD pattern of the pure wurtzite, the intensities of the (002) and (101) peaks are very different (Figure 7c, curve 5). In contrast, the JCPDS card of wurtzite (card no. 36-1450) indicates that the intensities of the two peaks are nearly equal. It is possible that there are preferred crystal orientations in the pure wurtzite, causing distinct difference between intensities of the two XRD peaks.

Because of the close similarity in the structures of sphalerite and wurtzite, many strong XRD peaks overlap (compare curves 1 and 5 in Figure 7c). Following the approach for the decomposition of XRD peaks developed in ref 42, we used the following method to separate the sphalerite (111) from the wurtzite (100), (002), and (101) peaks (Figure 7d). Because nanocrystalline ZnS particles are typically randomly oriented, we assumed that the intensities of the wurtzite (002) and (101) peaks are approximately equal. Each individual XRD peak was modeled using a Pearson VII equation. We set the fwhm of the wurtzite (002) peak to be the average of those of the wurtzite (100) and (101) peaks (based on the TEM data that indicate that the particles are equidimensional and because the 2θ separation of the peaks is small). Then, a nonlinear least-squares fit was performed to minimize the difference between the experimental XRD data and the sum of the Pearson VII curves of all XRD peaks under consideration (i.e., wurtzite (100), (002), and (101) peaks and sphalerite (111) peak). Fairly good fits were obtained for all standard samples (Figure 7c) and nanocrystalline ZnS samples (parts a and b of Figure 7), as demonstrated in Figure 7d. From the fitting, the intensity, fwhm, peak area, and the peak position (2θ) of every individual peak was obtained.

Figure 8a shows the correlation between the weight fraction of wurtzite (x_{wt}) in the standard samples with the area fraction (x_{Area}) of the wurtzite (100) or (002) peak. The area fraction of wurtzite equals the wurtzite peak area divided by the sum of the wurtzite peak area and the sphalerite (111) peak area. The correlation is nonlinear. The correlation between the wurtzite content and the (100) peak area fraction has a lower curvature than that for the (002) fraction. Thus, the latter correlation was used to calculate the wurtzite content of the heat-treated nanocrystalline ZnS samples. The correlation relation is repre-

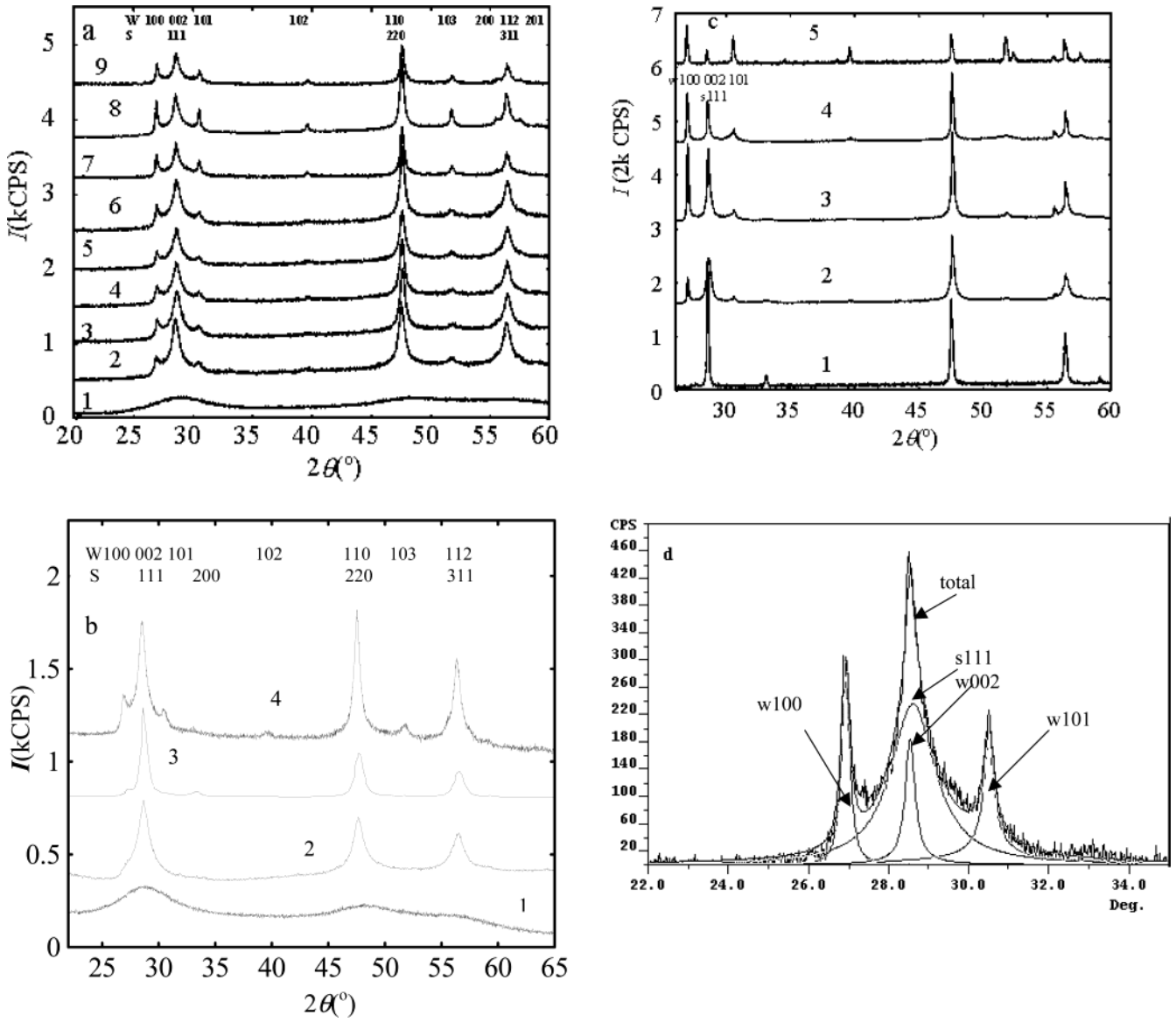

Figure 7. XRD patterns of ZnS samples collected at a scanning rate of 0.05 degrees/min (Cu Kα radiation, 35 kV, 40 mA). (a) Raw ZnS material (1), the material heated in silica tubes sealed under vacuum at 350 °C for 2 h (2), 500 °C for 9 h (3), 500 °C for 22 h (4), 500 °C for 48 h (5), 550 °C for 2 h (6), 750 °C for 1 h (7), 750 °C for 2 h (8), and 750 °C for 5 h (9). (b) Raw ZnS material (1), the material heated at 350 °C for 2 h in air (2), continued heating for additional 21 h (3), or in a silica tube sealed under vacuum (4). (c) A mixture of sphalerite and 0% (1), 25% (2), 50% (3), 75% (4), and 100% (5) wurtzite. (d) Decomposition of overlapping sphalerite and wurtzite peaks (see text). Principal sphalerite (S) and wurtzite (W) reflections are indicated above each graph. (Note: curve 3 in (b) was determined with Co Kα radiation using Bruker D8 Discover GADDS diffractometer but is plotted here against 2θ of Cu Kα wavelength for comparison.)

sented by the following equation obtained from nonlinear least-squares regression

$$x_{wt} = 1.6041(1 - 0.3752x_{Area(100)})x_{Area(100)} \qquad (11)$$

With the peak areas obtained from the peak decomposition method described above and the correlation eq 11, the weight fraction of wurtzite in each ZnS sample (Figure 7a) was calculated, as shown in Figure 8b. The average particle sizes of ZnS were calculated using the fwhms of the sphalerite (111) peak or the wurtzite (002) and (101) peaks according to the Scherrer equation (10), as shown in Figure 8c. In this Figure, the average particle size of wurtzite is the mean of the wurtzite dimensions along [001] and ⟨101⟩ . Relative standard deviations by repeated determinations are ∼7% for both phase content and average particle size.

Experimental Results and Discussion of Their Relevance to the MD Simulation Results. When the raw nanocrystalline ZnS (i.e., the initial synthesis product, predominantly sphalerite) was heated in a vacuum at 350 °C for 2 h, about 23% converted to wurtzite (Figure 8b). The average particle size of wurtzite formed was ∼9 nm, equal to the final sphalerite size. Heating at temperatures up to 750 °C increased the wurtzite content and average wurtzite particle size and caused a slight decrease in the average particle size of sphalerite. The decrease in sphalerite size can be attributed to the partial conversion of some particles to wurtzite (see Figure 6b). The wurtzite contents and the average particle sizes of ZnS at 500 °C changed little with reaction time. The slow kinetics at longer reaction times at 500 °C are in clear contrast to the fast transformation in the first 2 h at 350 °C.

We infer that the reaction at 500 °C slows down because the driving force for the growth of wurtzite becomes small as the wurtzite domains grow. The ∼21% wurtzite is distributed within sphalerite (Figure 6b). The width of remnant sphalerite domains

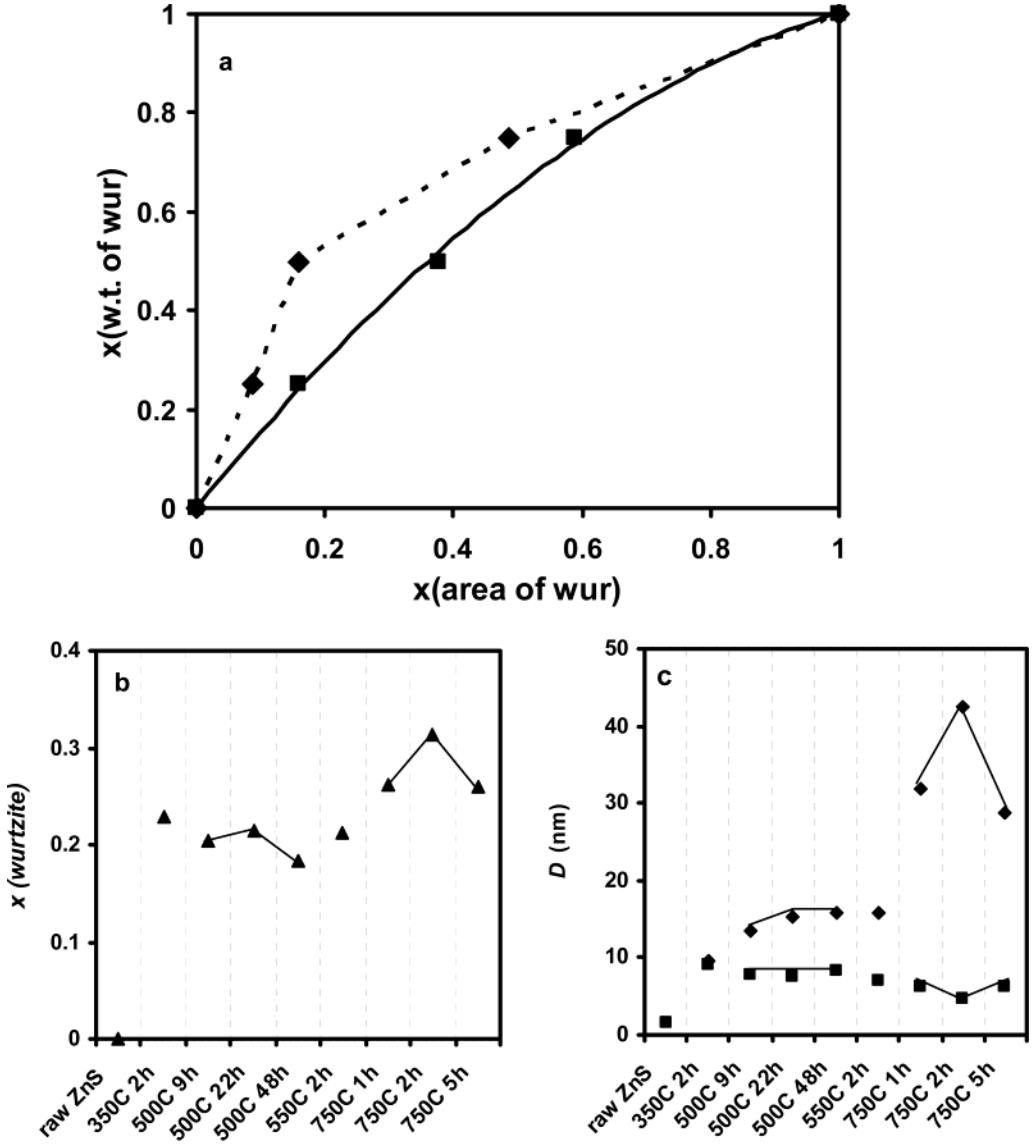

Figure 8. (a) Standard curve for correlation between weight fraction of wurtzite and the area fraction of wurtzite (100) peak (squares) or (002) peak (diamonds). The solid line is a regression curve; the dashed line connects data points only. (b) The weight fraction of wurtzite. (c) The average diameters of sphalerite (squares) and wurtzite (diamonds) in vacuum-sealed ZnS samples heated at different conditions.

is defined by the subdivision of the initial sphalerite particles by growth of wurtzite in the interior. Thus, with formation of sphalerite and wurtzite intergrowths, the relative stabilities of sphalerite and wurtzite are determined by the size of the domains of both phases. The data suggest that when the particle size of wurtzite is ∼15 nm and that of sphalerite ∼8 nm, the driving force for the transformation approaches zero. Eventually the transformation ceases because the whole nanoparticle cannot decrease its energy by growth of wurtzite. At 750 °C, the data points at 2 h show obvious deviations from those at 1 and 5 h, probably due to random errors in the XRD determination. Hence, the average wurtzite size at 750 °C overestimates the wurtzite size on the phase boundary, as shown in Figure 2b.

A plot of the average particle size of wurtzite formed in experiments at different times (after the initial rapid wurtzite growth phase) vs the temperature (data points in Figure 2b) shows good agreement with the phase boundary (solid line in Figure 2b) calculated by thermodynamic analysis. This supports the predictions from the MD modeling and confirms that sphalerite has a higher average surface energy than wurtzite. In contrast, the phase boundary (dotted line in Figure 2b) calculated using the surface energies from ref 17 shows significant deviation from the experimental data. We conclude that the surface energies (especially those of polar faces) calculated from static optimizations differ appreciably from actual values of real ZnS crystals at each temperature. Qadri et al. also observed the decrease in the transition temperature in nanocrystalline ZnS samples.[9] However, their observed average particle size of wurtzite is much larger than that observed in this work at the same temperature (Figure 2b).

Upon adsorption on ZnS nanoparticles, water strongly interacts with ZnS, causing relaxation of distorted surface structure and the release of the internal energy.[4] MD simulations show that the heat of adsorption of water on small ZnS nanoparticles is ∼500 kJ/mol of H_2O when the surface coverage of water is ∼1 H_2O/nm^2 of ZnS, indicating that water is strongly chemisorbed. Since sphalerite has higher average surface energy than wurtzite, the water−sphalerite interaction is stronger than that of water−wurtzite, and thus there is a greater energy decrease in the former than in the latter when enough water is adsorbed (Figure 5). This is consistent with preliminary results of our ongoing MD simulations of water adsorption on bulk ZnS, which show that the energy of sphalerite decreases ca. 5 times that of wurtzite when ∼2.5 H_2O molecules/nm^2 ZnS are

adsorbed on the (111) face of bulk sphalerite and the (001) face of bulk wurtzite. Thus, the sphalerite structure in nanoparticles becomes more stable than wurtzite when a sufficient amount of water is adsorbed, a phase stability inversion relative to ZnS nanoparticles in a vacuum. Because adsorbed water molecules could not be completely eliminated in air when the raw nano-ZnS sample was heated at 350 °C, wurtzite could not form readily (Figure 7b). The above conclusions may explain why natural ZnS nanoparticles[43] and ZnS nanoparticle samples synthesized in aqueous solutions are dominated by sphalerite.

Conclusions

Molecular dynamics simulations combined with thermodynamic analysis and experiments indicate that smaller ZnS nanoparticles in a vacuum are more thermodynamically stable in the wurtzite phase than in the sphalerite phase. The transition temperature from nanocrystalline sphalerite to wurtzite decreases dramatically as the average particle size decreases below ~20 nm. Water adsorption onto ZnS nanoparticles makes sphalerite more stable than wurtzite. Because of the ubiquity of water and water moisture in the environment, this conclusion is important for preparation and manipulation of desired nanocrystalline ZnS products. It is also key to the understanding of the formation, structure change, and transport of natural ZnS nanoparticles in our environment.

Acknowledgment. We thank Dr. W. Smith, Dr. T. R. Forester, and Dr. D. Fincham for providing MD simulations codes. Financial support for this work was provided by the U.S. Department of Energy (Grant # DE-FG03-01ER15218 and # LBNL LDRD 36615) and the National Science Foundation (Grant # EAR-0123967).

Supporting Information Available: Diagrams showing ZnS (100) surface relaxed and reconstructed by MD simulations at 300 K, calculated Wulff shape of a sphalerite ZnS crystal, and comparative study of MD simulations of water−ZnS nanoparticle with different water models. This material is available free of charge via the Internet at http://pubs.acs.org.

References and Notes

(1) Chen, R.; Lockwood, D. J. *J. Electrochem. Soc.* **2002**, *149*, S69.
(2) Nanda, J.; Sapra, S.; Sarma, D. D.; Chandrasekharan, N.; Hodes, G. *Chem. Mater.* **2000**, *12*, 1018−1024.
(3) Huang, F.; Zhang, H.; Gilbert, B.; Banfield, J. F. Surface State Controlled Nanocrystalline ZnS Structure Transformation. In *Abstracts of Papers*, 225th National Meeting of the American Chemical Society, New Orleans, LA, March 23−27, 2003; Oxford University Press: Cary, NC, 2003.
(4) (a) Zhang, H.; Gilbert, B.; Huang, F.; Banfield, J. F. *Nature* **2003**, *424*, 1025. (b) Gilbert, B.; Zhang, H.; Huang, F., Banfield, J. F. *Abstracts of Papers*, 225th National Meeting of the American Chemical Society, New Orleans, LA, March 23−27, 2003; Oxford University Press: Cary, NC, 2003.
(5) Barin, I.; Knacke, O.; Kubschewski, O. *Thermochemical Properties of Inorganic Substances*; Springer-Verlag: Berlin, 1977; pp 827−828.
(6) Desgreniers, S.; Beaulieu, L.; Lepage, I. *Phys. Rev. B* **2000**, *13*, 8726.
(7) Zhang, H.; Banfield, J. F. *J. Mater. Chem.* **1998**, *8*, 2073.
(8) McHale, J. M.; Auroux, A.; Perrotta, A. J.; Navrotsky, A. *Science* **1997**, *277*, 788.
(9) Qadri, S. B.; Skelton, E. F.; Hsu, D.; Dinsmore, A. D.; Yang, J.; Gray, H. F.; Ratna, B. R. *Phys. Rev. B* **1999**, *60*, 9191.
(10) Duran, J. D. G.; Delgado, A. V.; Gonzalez-Caballero, F. *Mater. Chem. Phys.* **1994**, *38*, 42.
(11) Cammarata, R. C.; Sieradzki, K. *Annu. Rev. Mater. Sci.* **1994**, *24*, 215.
(12) Nosker, R. W.; Mark, P.; Levine, J. D. *Surf. Sci.* **1970**, *19*, 291.
(13) Yoshiyama, H.; Tanaka; Mikami, Y.; Ohshio, S.; Nishiura, J.; Kawakami, H.; Kobayashi, H. *J. Cryst. Growth* **1988**, *86*, 56.
(14) Tauson, V. L.; Abramovich, M. G. *Physicochemical Transformation of Real Crystals in Mineral Systems*; Novosibirsk: Izdvo "Nauka", Sibirskoe Otdnie, 1988; p 121.
(15) Lindan, P. J. D.; Harrison, N. M.; Gillan, M. J.; White J. A. *Phys. Rev. B* **1997**, *55*, 15919.
(16) Wright, K.; Watson, G. W.; Parker, S. C.; Vaughan, D. J. *Am. Mineral.* **1998**, *83*, 141.
(17) Hamad, S.; Cristol, S.; Catlow, C. R. A. *J. Phys. Chem. B* **2002**, *106*, 11002.
(18) Tauson, V. L.; Abramovich, M. G. *Mineral. Zh.* (Russian) **1982**, *4*, 35.
(19) Tauson, V. L.; Abramovich, M. G.; Akimov, V. V.; Scherbakov, V. A. *Geochim. Cosmochim. Acta* **1993**, *57*, 815.
(20) Duke, C. B. *Chem. Rev.* **1996**, *96*, 1237.
(21) Rustad, J. R.; Dzwinel, W.; Yuen, D. A. Computational Approaches to Nanomineralogy. In *Reviews in Mineralogy & Geochemistry, Nanoparticles and the Environment*; Banfield, J. F., Navroitsky, A., Eds.; Mineralogical Society of America and Geochemical Society: Washington, DC, 2001; Vol. 44.
(22) Iglesias, O.; Labarta, A. *Phys. Rev. B* **2001**, *63*, 184416.
(23) Averback, R. S.; Zhu, H.; Tao, R.; Hofler, H. Sintering of nanocrystalline materials: experiments and computer simulations. In *From Synthesis and Processing of Nanocrystalline Powders*; Bourell, D. L., Ed.; The Minerals, Metals, and Materials Society: Warrendale, Pennsylvania, 1996.
(24) Ogata, S.; Iyetomi, H.; Tsuruta, K.; Shimojo, F.; Nakano, A.; Kalia, R. K.; Vashishta, P. *J. Appl. Phys.* **2000**, *88*, 6011.
(25) Liu, B. X.; Lai, W. S.; Zhang, Z. J. *Adv. Phys.* **50**, 367, 2001.
(26) Kostov, I.; Kostov, R. I. *Crystal Habits of Minerals*; Prof. Marin Drinov Academic Publishing House & Pensoft Publishers: Sofia, 1999; pp 114−120.
(27) Wright, K.; Jackson, A. *J. Mater. Chem.* **1995**, *5*, 2037.
(28) Benkabou, F.; Aourag, H.; Certier, M. *Mater. Chem. Phys.* **2000**, *66*, 10.
(29) Dick, B. G.; Overhauser, A. W. *Phys. Rev.* **1958**, *112*, 90.
(30) Smith, S.; Forester, T. R. *The DL-Poly2 User Manual*; Daresbury Laboratory: Daresbury, Warrington, U.K., 2001; version 2.13.
(31) Fincham, F. *Shell-Dynamo Reference Manual*; University of Keele: Keele, Staffordshire, U.K., 1996.
(32) Mineral Physics & Crystallography. *A Handbook of Physical Constants*; Ahrens, T. J., Ed.; American Geophysical Union: Washington, DC, 1995.
(33) Chen, W., Kahn, A.; Soukiassian, P.; Mangat, P. S.; Gaines, J.; Ponzoni, C.; Olego, D. *J. Vac. Sci. Technol., B* **1994**, *12*, 2639.
(34) *Reviews in Mineralogy & Geochemistry, Molecular Modeling Theory: Applications in the Geosciences*; Cygan, R. T., Kubicki, J. D., Eds.; Geochemical Society and Mineralogical Society of America: Washington, DC, 2001; Vol. 42.
(35) de Leeuw, N. H.; Parker, S. C. *Phys. Rev. B* **1998**, *58*, 13901.
(36) Berendsen, H. J. C.; Grigera, J. R.; Straatsma, T. P. *J. Phys. Chem.* **1987**, *91*, 6269.
(37) Stillinger, F. H.; Rahman, A. *Chem. Phys.* **1978**, *68*, 666.
(38) Harris, D. J.; Brodholt, J. P.; Harding, J. H.; Sherman, D. M. *Mol. Phys.* **2001**, *99*, 825.
(39) Stevens, J. E.; Chaudhuri, R. K.; Freed, K. F. *J. Chem. Phys.* **1996**, *105*, 8754.
(40) Huang, F.; Zhang, H.; Banfield, J. F. *Nano Lett.* **2003**, *3*, 373.
(41) Jenkins, R.; Snyder, R. L. *Introduction to X-ray Powder Diffractometry*; John Wiley & Sons: New York, 1996; p 90.
(42) Zhang, H.; Banfield, J. F. *J. Phys. Chem. B* **2000**, *104*, 3481.
(43) Labrenz, M.; Druschel, G. K.; Thomsen-Ebert, T.; Gilbert, B.; Welch, S. A.; Kemner, K. M.; Logan, G. A.; Summons, R. E.; Stasio, G. D.; Bond, P. L.; Lai, B.; Kelly, S. D.; Banfield, J. F. *Science* **2000**, *290*, 1744.